Optical absorption from an indirect transition in bismuth nanowires

M. R. Black,[1,*] P. L. Hagelstein,[1] S. B. Cronin,[2] Y. M. Lin,[1] and M. S. Dresselhaus[1,3]
[1]*Department of Electrical Engineering and Computer Science, Massachusetts Institute of Technology, Cambridge, Massachusetts 02139-4307, USA*
[2]*Department of Physics, Harvard University, Cambridge, Massachusetts 02138, USA*
[3]*Department of Physics, Massachusetts Institute of Technology, Cambridge, Massachusetts 02139-4307, USA*
(Received 26 April 2003; published 30 December 2003)

Simulations of the optical absorption in bismuth nanowires resulting from an indirect interband L-T-point transition are presented. The absorption dependence at room temperature on the band overlap, effective masses, and wire diameter is explored. The polarization, wave number, and wire size dependence of the high intensity absorption peak observed in bismuth nanowires at $\sim$1000 cm^{-1} can be explained by our model. The polarization dependence of the optical absorption arises from a surface component of the optical coupling term which enhances this indirect transition. Simulations of the absorption from a valence-band L-T-point transition correctly predict the magnitude of the increase in the peak energy (wave number) with decreasing wire diameter. The wave numbers of the simulated and measured absorption peaks differ by $\sim$400 cm^{-1}. Several explanations for this discrepancy are proposed.

DOI: 10.1103/PhysRevB.68.235417 PACS number(s): 78.67.Lt, 73.50.Dn, 73.61.At

I. INTRODUCTION

A better understanding of the electrical transport and the optical absorption inside bismuth nanowires will help to utilize the unusual properties of these nanowire arrays for optical[1] and thermoelectric[2] applications. One aspect of the electronic structure of bismuth that makes bismuth nanowires especially promising for these applications is the low effective mass of its electron carriers. Bismuth, in bulk form, is a semimetal with a small band overlap (38 meV at 5 K) and a very anisotropic electron effective-mass tensor (varying from $0.001m_0$ to $0.26m_0$ at low temperatures, depending on the crystalline direction).[3] For a Bi nanowire with a small enough wire diameter, d_w, and hence significant quantum confinement, the nanowire undergoes a transition from a semimetal with a small band *overlap* to a semiconductor with a small indirect *band gap*, thus allowing the unusual properties of bismuth to be available as a semiconducting material as well as a semimetal. This transition, as well as other quantum effects, occurs in Bi nanowires at relatively large wire diameters because of the small effective mass and small band overlap of bulk bismuth. For example, in nanowires oriented along the $\langle 012 \rangle$ crystalline direction (such as the wires on which the optical measurements of this study were made[4]), this transition is predicted to occur[5] at a diameter of 49 nm at 77 K and 13 nm at 293 K.

Bismuth nanowires have a strong absorption peak in the midinfrared (mid-IR) that is not present in bulk bismuth. Figure 1 compares the optical reflection spectra of a thin film of bismuth with that of free-standing bismuth nanowires. The dominant feature in this energy range for the bismuth nanowires is at $\sim$1000 cm^{-1}. This feature is not present in the corresponding spectrum for a bismuth film. The absorption spectra of bismuth nanowires can be separated into one large and several small intensity peaks.

In bismuth nanowires, many mechanisms are expected to contribute to the optical absorption within the same energy range. For example, intersubband, direct interband, and indirect interband transitions all occur in the midinfrared energy range. Separating the effects of the different absorption mechanisms from each other is difficult, and therefore requires theoretical modeling of each mechanism. In previous studies of the optical absorption of bismuth nanowires, the contributions to the optical absorption from both intersubband and direct interband transitions were modeled, and the results were compared to the measured absorption spectra.[1] The theory for the absorption resulting from a direct interband transition in bismuth nanowires did not show agreement with the experimentally measured data. However, the theory presented for optical absorption resulting from intersubband transitions did predict the observed energy at which the optical-absorption peaks should occur, the polarization dependence of the absorption, and the qualitative diameter dependence of the absorption peak energy.[1,6] The smaller

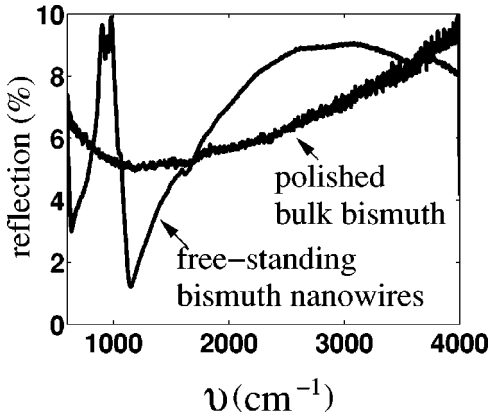

FIG. 1. Wave-number dependence of the reflection, $R(\nu)$, of a polished piece of bulk bismuth and of free-standing nanowires. The large feature near $\sim$1000 cm^{-1} in the reflection spectra of the free-standing wires is not present in the reflection spectra of bulk bismuth. The broad features in the bulk bismuth reflection spectrum are likely a result of a nonperfect polish or of a misalignment with the optical stage.

intensity absorption peaks were thus attributed to optical absorption resulting from intersubband transitions, but the intersubband theory did not completely explain the large peak near 1000 cm^{-1}. The magnitude of the energy shift of this peak with a change in wire diameter, as well as the overall shape of the absorption spectra near this absorption peak, were not explained by either of the previously published models.[1,6] In addition, the absorption peak at $\sim$1000 cm^{-1} has a much larger intensity in the experimentally observed spectra than the features identified with the intersubband transitions in the previous work. The previously published paper, therefore, concluded that intersubband transitions could account for the weaker features, but that another absorption mechanism was needed to explain the strong sharp peak in the absorption spectra of bismuth nanowires in the mid-IR energy range.[1] The present paper addresses the additional and important role of indirect transitions in the optical properties of bismuth nanowires.

In this paper, we present a model for an indirect transition that, in combination with the previously published model for the intersubband transitions, can explain the observed absorption spectra. Section II explains qualitatively why this indirect transition needs to be considered. Section III presents a detailed study and numerical simulations of the optical absorption of bismuth nanowires resulting from this indirect transition. In Sec. IV, the theoretical results are compared to the measured spectra. Conclusions are given in Sec. V.

II. A QUALITATIVE PICTURE OF THE INDIRECT TRANSITION

The qualitative wire diameter and polarization dependences, as well as the energy (wave number) of the absorption peak at $\sim$1000 cm^{-1}, strongly suggest that this absorption is from intersubband transitions. However, the absorption resulting from indirect intersubband transitions can, in principle, also explain a large absorption peak at $\sim$1000 cm^{-1}. Often indirect transitions are weaker than direct transitions, since a phonon is required for conservation of momentum. However, since the Debye temperature of bismuth[7] is only 86.5–112 K, many phonons are available at room temperature to contribute to an indirect transition in a phonon absorption process.

In bulk bismuth, carrier pockets are located at both the *L* and the *T* points. Near the Fermi level, the *L* point has both valence and conduction bands which are a mirror image of each other and are separated by a small energy gap of 36 meV at room temperature.[8] The *L*-point bands are highly nonparabolic and are approximated by the Lax two-band model.[10] The effective-mass tensor at the band edge at the *L* point has very small effective-mass components and is highly anisotropic (varying from about $0.006m_0$ to $1.4m_0$ at room temperature, depending on the crystalline direction[8]). The highest *T*-point valence band is parabolic with the hole carrier pocket having, in general, a larger effective mass than the *L*-point carriers, varying from about $0.059m_0$ to $0.634m_0$ at 1.7 K depending on the crystalline direction,[3] see Fig. 2.

Since bulk bismuth is a semimetal, the Fermi energy crosses the *T*-point valence band, creating many unoccupied electronic states (holes). The *L*-point valence band, however, is 90 meV below the Fermi energy and is therefore mostly filled at room temperature. Since the two types of valence bands track each other approximately (have similar shifts in energy with varying momentum), as in the case of intersubband transitions, and since the initial *L*-point valence band is fully occupied while the final *T*-point valence band is partially unoccupied, we expect a strong indirect *L*-*T*-point absorption over a narrow wave-number range, provided that momentum is conserved, as discussed below.

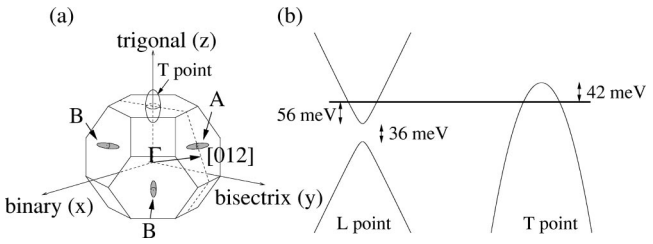

FIG. 2. (a) Brillouin zone of bismuth showing the *T*-point hole pocket and the three *L*-point electron pockets, labeled "*A*" and "*B*" (doubly degenerate in our wires). (b) The dispersion relations of the *L*-point and *T*-point bands shown schematically. From the literature, the *L*-point band gap is 36 meV (Ref. 8), the *L*-point electron Fermi energy is 56 meV (Ref. 9), and the *T*-point hole Fermi energy is 42 meV at room temperature (Ref. 9).

Both the *L*- and *T*-point valence bands exhibit significant quantum confinement for the bismuth nanowire diameters used in this study. Since the *L*-point carriers have, in general, a smaller effective mass than the *T*-point carriers, the subbands at the *L* point are separated by a larger energy difference than those at the *T* point. In other words, with decreasing wire diameter, both the *L*- and *T*-point valence bands move down in energy, but the *L*-point valence bands move down at a faster rate than the *T*-point valence bands. The energy of the indirect transition from the *L*- to the *T*-point valence bands is therefore expected to increase with decreasing wire diameter, but not as rapidly as for a direct interband or an intersubband transition. Experimental measurements show[6] that when the wire diameter is decreased from 80 to 35 nm, the wave number of the absorption peak increases by 65 cm^{-1}. The theory of intersubband transitions in bismuth nanowires predicts an increase in the wave number of the absorption peak measured in wave numbers by $\sim$900 cm^{-1} at room temperature for a wire diameter change from 80 to 35 nm. However, since the energy (wave-number) shift of the absorption peak from an indirect *L*-*T*-point valence-band transition is determined mainly by the difference between the two effective masses, and not so much by the values of the effective masses themselves, this shift with wire diameter is much less for the indirect *L*-*T* transition than for the direct *L*-point transition, and the *L*-*T* transition energy fits much better with the experimental measurements on the wire diameter dependence of the peak energy. As the wire diameter decreases from 70 to 35 nm, the simulations for the indirect transition predict a modest increase in the absorption peak energy (measured in wave numbers) by only

$\sim 100\ \mathrm{cm}^{-1}$, close to the experimentally observed shift, as discussed below.

The optical absorption at $\sim 1000\ \mathrm{cm}^{-1}$ has a very strong polarization dependence.[6] When light is polarized perpendicular to the wire axis, the absorption versus wave number has a strong sharp feature at $\sim 1000\ \mathrm{cm}^{-1}$. As the polarization angle is rotated away from the normal to the wire axis, the intensity of this feature decreases, and eventually, for light polarized parallel to the wire axis, this absorption peak disappears.[6] This polarization trend agrees with the selection rules for intersubband absorption and is one reason why the strong absorption peak at $\sim 1000\ \mathrm{cm}^{-1}$ was initially attributed to an intersubband absorption.[6] However, the polarization dependence can also be explained by an indirect transition enhanced by surface effects.[11] One explanation for why an indirect transition would be enhanced by surface effects is that proposed by Miller *et al.* They predicted an enhancement of indirect transitions at the interface between two materials having a dielectric constant mismatch due to a surface contribution to the optical matrix element given by the following argument.[11]

The optical transition matrix element M_e is composed of two terms,

$$M_e = \langle \Psi_{\mathrm{final}} | A \cdot \nabla + \nabla \cdot A | \Psi_{\mathrm{initial}} \rangle. \tag{1}$$

The first term, $\langle \Psi_{\mathrm{final}} | A \cdot \nabla | \Psi_{\mathrm{initial}} \rangle$, is used to calculate the optical matrix element in bulk solids. The second term, $\langle \Psi_{\mathrm{final}} | \nabla \cdot A | \Psi_{\mathrm{initial}} \rangle$, results from the spacial derivative of the vector potential, and in a homogeneous material (for one commonly used gauge of A) this term is zero. In contrast, the wavelength of light is much larger than the wire diameter. For the gauge of A that gives a zero $\nabla \cdot A$ value for a bulk material, a nonzero value results at the interface between two materials with different dielectric constants, for example at the bismuth/alumina interface in our nanowires.[11,12] Furthermore, since the dielectric function does not instantaneously change at the interface, but instead changes throughout a distance d_{pd}, and since the wire diameter is small, this change could occur throughout most of the wire radius.

In the case of a large surface interface area, as in bismuth nanowires, the surface matrix element term cannot be ignored. Miller *et al.* found experimentally that the surface contribution to the matrix element enhances the indirect transition in their gold samples.[11] In another study, Enders and Schuchardt observed an increase in the amplitude of the dielectric function of bismuth with the addition of antimony.[13] They attributed the increase in the dielectric function to an enhanced indirect transition in bismuth resulting from the short-range scattering potential of the Sb dopant sites. In bismuth nanowires, since bismuth has a significant index of refraction [$n = 2.6$ at $1000\ \mathrm{cm}^{-1}$ (Ref. 3)], both bismuth/alumina ($n = 1.7$) and bismuth/air ($n = 1$) have significant dielectric constant mismatches, and therefore the surface contribution to the matrix element is significant.

If the strong optical absorption at $\sim 1000\ \mathrm{cm}^{-1}$ is a result of the surface enhancement of the optical matrix element, this absorption should have a large polarization dependence. When the light is polarized such that the electric field crosses an interface perpendicular to the wire axis, the surface term is nonzero. However, when the electric field of the incident light is parallel to the wire axis, the surface term should be zero since the electric field does not cross a bismuth/air (or alumina) boundary.

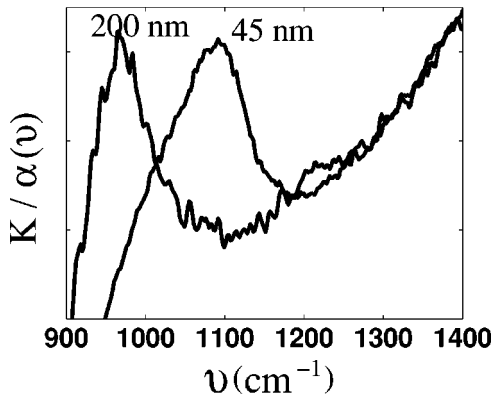

FIG. 3. The wave-number dependence of the imaginary part of the index of refraction, $K(\nu)$, of 200 nm and of the absorption coefficient, $\alpha(\nu)$, of $\sim$45-nm-diam bismuth nanowires fabricated inside an alumina template but with this template then removed. The absorption peak of the 200- and $\sim$45-nm wire diameter samples are at 965 and 1090 cm^{-1}, respectively. The imaginary part of the index of refraction of the 200-nm-diam wires was obtained by Kramers-Kronig relations and measurements of the optical reflectivity of the sample. The absorption of the $\sim$45-nm-diam wire was obtained from the negative log of the transmission of the sample. The absorption values are not corrected for surface roughness or sample thickness, and so the *y*-axis scales for the two graphs are different and arbitrary.

This argument has additional credibility since the reflection of a roughed-up bulk bismuth sample also has a feature at around $\sim 1000\ \mathrm{cm}^{-1}$. In addition, the thin film of bismuth that was used to provide a background spectrum in a previously published paper[1] also shows a shallow feature in the transmission at $\sim 1000\ \mathrm{cm}^{-1}$, but it is broader and weaker. The feature in the thin-film bulk bismuth sample likely results from some small surface roughness inherent in the thin-film fabrication. Furthermore, even though 200-nm-diam bismuth wires are too large to show significant quantum confinement, they still show an absorption peak at $965\ \mathrm{cm}^{-1}$. The 200-nm-diam wires and their absorption peak at $965\ \mathrm{cm}^{-1}$ are, therefore, characteristic of crystalline bulk (not quantum confined) bismuth with a large surface area. Figure 3 shows the wave-number dependence of the absorption coefficient, $\alpha(\nu)$, obtained by the Kramers-Kronig relations of the reflectivity of 200-nm-diam, free-standing, bismuth wires. For comparison, the figure also shows the imaginary part of the index of refraction, K, of $\sim$45-nm-diam wires, obtained by taking the negative log of their measured transmission. The 200-nm-diam wires have an absorption peak at a wave number of about $125\ \mathrm{cm}^{-1}$ less than the $\sim$45-nm wire diameter sample. Since rough bulk samples, thin films, and 200-nm-diam wires all show an absorption peak around $\sim 1000\ \mathrm{cm}^{-1}$, this strong absorption peak likely results from the indirect L- to T-point transition and not from intersubband transitions, in agreement with the

argument discussed above regarding the diameter dependence of the strong, sharp, absorption peak.

III. THEORY AND NUMERICAL SOLUTIONS OF THE OPTICAL ABSORPTION FROM AN *L*-*T*-POINT INDIRECT ELECTRONIC TRANSITION

Model calculations are presented in order to understand the indirect L-T transition in bismuth nanowires, and hence to gain insight into the mechanism responsible for the absorption peak(s) observed in the experimental data. For this work, a phonon-assisted process is assumed, although one possibility is that the indirect transition is assisted by a surface defect at the bismuth-oxide interface. Since a surface defect is localized in real space, it is distributed in momentum space, and therefore a phonon might not be required if the surface state couples the initial and final states.

A photon can excite an electron to an unfilled higher-energy state if the energy of the photon exactly equals the energy difference between the final and the initial states (plus or minus the energy of a phonon in an indirect process) and if momentum is conserved. The photon absorption from this process can be measured by energy-dependent optical-absorption spectra. In order to conserve momentum in an indirect transition, a phonon with momentum equal to the momentum difference between the final and initial states must be absorbed (or emitted). The optical-absorption coefficient $\alpha_{L\text{-}T}$ resulting from an indirect electronic excitation from the L-point valence band to the T-point valence band in a Bi nanowire as a function of photon energy, $\hbar\omega$, is given by

$$\begin{aligned}\alpha_{L\text{-}T}(\omega) \propto & \sum_{p=1,2,3} \sum_{n} \sum_{m} \int dk_n \int dk_m N_{\mathrm{ph}}(E) \times M_e(n,m)^2 \\ & \times \{f[E_n(k_n)] - f[E_m(k_m)]\} \\ & \times \delta(E_m(k_m) - E_n(k_n) \pm E_{\mathrm{phonon}} - \hbar\omega) \\ & \times \delta(k_m - k_n \pm k_{\mathrm{phonon}}), \end{aligned} \tag{2}$$

where ω is the frequency of the incident light, p is 1, 2, or 3 corresponding to the three L-point hole pockets, n and m are the L-point and T-point subband indices, respectively, k_n and k_m are the wave vectors of the L- and T-point valence-band states in the direction of the wire axis, N_{ph} is the phonon population described by the Planck distribution function, $M_e(n,m)$ is the momentum matrix element coupling strength between the initial, n, and final, m, subbands, $f(E_n)$ and $f(E_m)$ are the Fermi-Dirac distribution functions for the states n and m, respectively, and E_n and E_m are the corresponding energies of states n and m. In Eq. (2), the momentum of the incident photon is ignored, since it is much less than the momentum of the phonon, and the electron-phonon coupling strength is, for simplicity, assumed to be constant.

In our calculations, the acoustic phonons are modeled using the Debye model so that the velocity of sound c_s is taken as a constant of 2.54×10^3 m/s.[3] The simulation results are found to be insensitive to the velocity of sound. Since the L-point bands are strongly coupled, the Lax two-band model for nonparabolic coupled bands is used to describe the dispersion relations.[14] Since the L-point electronic bands are extremely anisotropic and show strong nonparabolic effects, the calculation of the wave functions is done numerically. The Fermi energy as well as the energy levels and wave functions for the first 50 subbands are found by a modified version of a previously published model of the electronic structure,[5] the modified version taking into account the nonparabolic dispersion relations of the subbands in calculating the Fermi energy. The model takes as variables the wire crystallographic orientation along the wire axis, the wire diameter, and the temperature. For all calculations in this work, unless otherwise stated, the wires are assumed to be undoped, so that the Fermi energy is set to ensure charge neutrality.

The matrix element $M_e(n,m)$ is calculated by assuming a penetration depth d_{pd} of the surface component of the matrix element in Eq. (1) and by calculating the integral

$$M_e(n,m) = \int \psi_n \exp\left(-\frac{(R_0 - r)}{d_{\mathrm{pd}}}\right) \psi_m dr d\theta, \tag{3}$$

where R_0 is the radius of the nanowire, and the integral is taken over the cross-sectional area of the wire, $dr d\theta$, and ψ_n and ψ_m are the wave functions of states n and m, respectively. Various matrix elements were tried, including coupling of the initial and final states through an intermediate surface state. All methods gave very similar results. Hence, the simplest version is presented here.

The penetration depth of the surface matrix element, d_{pd}, is varied to better fit the experimental data. When the penetration depth is large compared to the wire diameters, Eq. (3) reduces to a spatial overlap of the wave functions. Unlike the case of intersubband transitions,[1] when the spacial overlap is used as the matrix element, one initial T-point subband state usually couples strongly to only one (or at most three) L-point subband state(s). In addition, because of the differences in the effective-mass tensors at the T and L points, the lower-order T-point subbands couple more strongly to an L-point subband than higher-order T-point subbands do. In other words, the first T-point subband will couple strongly with only the first L-point subband, while the tenth T-point subband will couple most strongly with the tenth L-point subband, and the coupling between the first states will be stronger than between the tenth states.

As the penetration depth d_{pd} of the surface component of the matrix element decreases, each T-point subband state couples to more L-point subbands. In addition, for smaller penetration depths, higher-order states couple more strongly than lower-order states since their wave functions are on average closer to the boundary of the wire. Both these trends lead to a broader absorption peak. In addition, as the decay length is decreased, the smaller wire diameter wires absorb more strongly than the larger diameter wires, since they have a larger surface area to volume ratio. The smaller the diameter of the wires, the less volume an individual wire occupies, however for a given sample size, the smaller the wire the more wires are simultaneously measured, and so the volume measured is roughly independent of the wire diameter.

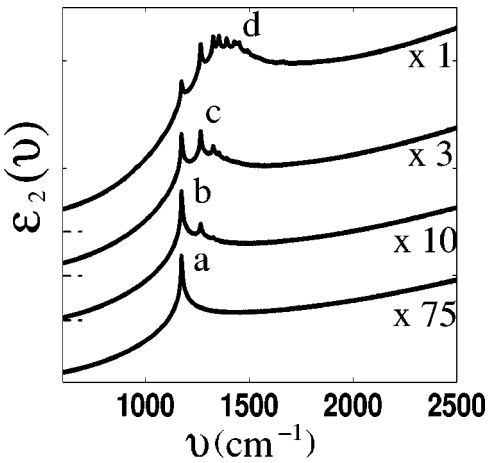

FIG. 4. The calculated absorption spectra, plotted in terms of ϵ_2, resulting from electronic transitions from pocket *A* at the *L* point to the *T* point, assuming a phonon absorption process. The matrix elements $M_e(n,m)$ are scaled by Eq. (4) with *s* set to 1, 0.5, 0.25, and 0.1 for graphs *a*, *b*, *c*, and *d*, respectively. The curves *b*, *c*, and *d* are offset with respect to the dotted lines and are multiplied by 75, 10, and 3, respectively.

Hence, an increase in the surface area to volume ratio increases the absorption intensity.

Even for the limiting case of $d_{\mathrm{pd}} \gg d_w$, where d_w is the wire diameter, the experimental spectra have a narrower absorption peak than the simulated spectra. This discrepancy could indicate that the higher-order subbands are not well defined in the wires, for example because of limits in the infinite barrier approximation or because of surface roughness on the wires. The discrepancy could also result from limitations of the two-band model assumed in this calculation. Instead of fitting d_{pd} to the linewidth of the spectrum, d_{pd} is fit to the ratio of the intensities of the experimentally observed absorption peak for 35-nm and 60–80-nm-diam wires.[6] Using this method, d_{pd} is found to be 15 nm.

In order to determine the dependence of the peak width on the number of subbands that were included in the simulation, the matrix element was multiplied by a decaying exponential function with a dependence on the subband numbers of the initial, *n*, and the final, *m*, states,

$$M_e(n,m) \rightarrow M_e(n,m)\exp(-sn)\exp(-sm), \qquad (4)$$

where *s* is a fitting coefficient. The curves *a*, *b*, *c*, and *d* in Fig. 4 show the calculated imaginary part of the dielectric function, ϵ_2, with *s* chosen to be equal to 1, 0.5, 0.25, and 0.1, respectively. The absorption spectra show contributions to the absorption resulting from electrons only in pocket *A*, see Fig. 2(a), and are only for the phonon absorption process (simulations of the phonon emission process would result in similarly shaped absorption spectra at an energy 160 cm^{-1} higher), as discussed below. The larger the value of *s*, the more the lower-order subbands dominate the absorption spectra. When the lower-order subbands dominate the absorption spectra, the absorption peak is narrower and occurs at a lower energy [1174 cm^{-1} for $s=1$ (a) versus 1380 cm^{-1} for $s=0.1$ (d) and 1540 cm^{-1} for $s=0$ (not shown)] than when higher-order subbands also contribute significantly to the absorption spectra. In this paper, for all the spectra that are presented, except those in Fig. 4, the approximation $s=0$ was taken in order to minimize the number of fitting parameters and simplify the data analysis. Therefore, the lower-order subbands are not favored in the present calculation.

Unlike the case of intersubband transitions,[1] even with $s=0$, the higher-order subband states do not contribute significantly to the absorption coefficient for the indirect transition process described here. For example, in a 35-nm-diam wire, the 20th *T*-point valence band is more than 60 meV below the Fermi energy. Since an empty state near the *T* point is required for the indirect absorption, and since the higher-level subbands are mostly filled, only the first 20 subbands at the *T* point are considered in the calculation. Since higher-level subbands at the *L* point couple only weakly to the first 20 subbands at the *T* point, only the first 20 subbands at the *L* point are considered. In addition, surface conditions and possibly limitations to the two-band model will likely limit the number of well-defined subbands. The contribution to the optical absorption from electronic transitions between the first 15 *T*-point and the first 15 *L*-point subbands of pocket *A* in 35-nm-diam bismuth wires at 293 K is shown in Fig. 5(a). Only those transitions with significant coupling strength are shown. The figure shows that after the first nine subband transitions, the intensities of the absorption peaks sharply decrease.

Figure 5(b) shows the energy difference of the band edges as a function of subband number in wave numbers for pocket *A*. Since the *L*-point and *T*-point masses are different, the energy difference between the *L*- and *T*-point band edges also varies as the subband number is varied. Each transition, therefore, has a slightly different absorption peak wave number, thereby contributing to the linewidth of the peak. Since the *L*-point effective mass increases with energy due to nonparabolic effects, the effective masses (in the confined direction) of the *L*-point subbands also increase with increasing subband index. When the effective mass (in the confined directions) of the *L* point equals the effective mass of the *T* point, the two bands decrease in energy at the same rate as the subband number is increased. Therefore, at this point, many transitions have the same energy difference between them, thus resulting in a large contribution to the absorption peak. From Fig. 5(b) we see that for states 8–20, the energy difference between the subbands is fairly constant, and thus the absorption peaks from these subbands all contribute to the observed optical absorption at nearly the same energy. The transitions from subbands where the effective masses of the *L* and *T* points are different contribute to the linewidth of the absorption spectra.

The contributions to the absorption spectra associated with the indirect transition from the three *L*-point pockets (one *A* pocket and two *B* pockets) to the *T*-point hole pocket are shown in Fig. 6. For $\langle 012 \rangle$ aligned Bi wires (such as our wires), two of the three electron pockets are degenerate. The two degenerate pockets are labeled "pocket *B*" in Fig. 6, and the third nondegenerate electron pocket is labeled "pocket *A*." For each pocket, the absorption spectrum has two distinctive absorption peaks, one (at higher energy) for the

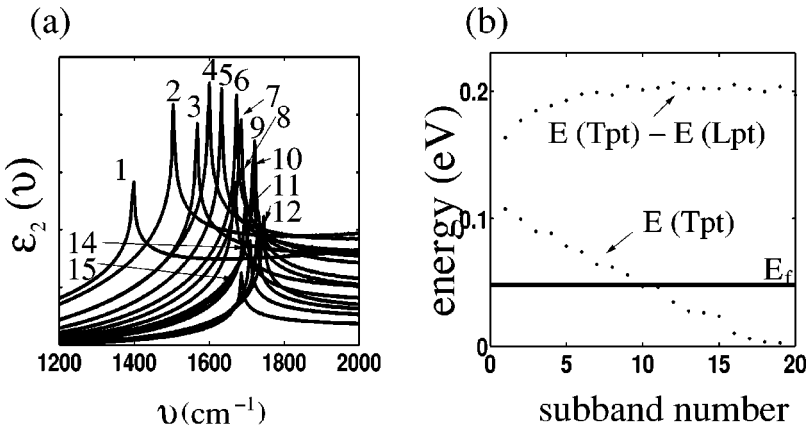

FIG. 5. (a) The simulated optical absorption from transitions from the first 15 *T*-point subbands to their corresponding *L*-point subbands for one pocket of an undoped, 35-nm-diam bismuth nanowire at 293 K. As the *T*-point subband index is increased, the absorption intensity decreases, since the higher subbands at the *T* point have fewer empty states to which an electron from the *L* point can be excited. The wave number of the absorption peak increases rapidly with increasing subband number until about the tenth state, at which point it levels off and eventually slowly decreases. (b) The energy difference between the band edges of the *L*- and *T*-point valence bands, the Fermi energy, and the energy of the *T*-point band edge as a function of the state or subband number.

emission of a phonon and one (at lower energy) for the absorption of a phonon. The peaks for each process are shown separately as well as the total contribution to the absorption from both processes. Pocket *A* has a larger intensity absorption peak than pocket *B*, since the effective-mass components in the confined directions of this pocket are better matched to those at the *T* point. The more closely the effective-mass components in the confined directions of the initial and final states are matched, the greater the number of subbands that contribute to the absorption at the same energy, and hence the absorption peak is enhanced.

Since the electronic band parameters at room temperature are not accurately known, we considered the sensitivity of our model to variations of the band parameters. First we consider variation of the band overlap and then variation of the effective-mass components. Figure 7 shows the calculated absorption spectra with varying values of the bulk bismuth band overlap energy of the *L* and *T* points used in the simulations. Curve II is for the measured band overlap of 98 meV (790 cm^{-1}) for bulk bismuth,[9] and curves I and III are for a band overlap of $98+74$ meV (1387 cm^{-1}) and $98-74$ meV (194 cm^{-1}), respectively. Values of the band overlap were chosen so that the change in the absorption spectra was significant, and so that the lower band overlap energy of 24 meV resulted in an absorption peak near the energy of the observed absorption peak, as discussed below. An increase (decrease) in the band overlap energy results in an upshifted (downshifted) absorption peak energy by the same amount.

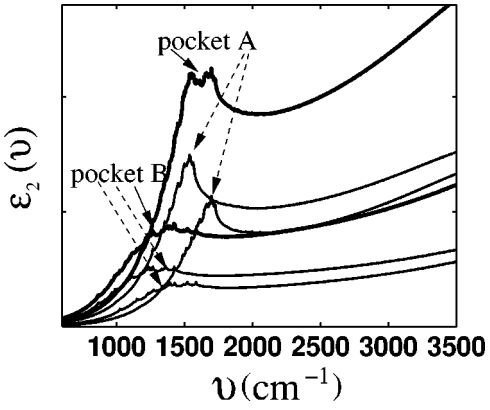

FIG. 6. The calculated absorption spectra from the nondegenerate hole pocket *A* and the doubly degenerate hole pocket *B* at the *L* point, see Fig. 2, to the *T*-point valence band of a 45-nm-diam ⟨012⟩ aligned bismuth nanowire at room temperature. The absorption is plotted in terms of the wave-number dependence of the dielectric function $\varepsilon_2(\nu)$. Each pocket has two absorption peaks, one when a phonon is emitted (at higher ν) and one when a phonon is absorbed (at lower ν). The total absorption (solid arrows) as well as the absorption assuming just phonon emission or just phonon absorption (dotted line arrows) are shown.

The energy of the absorption peak is not only sensitive to the energy overlap of the *L*- and *T*-point bands, but is also

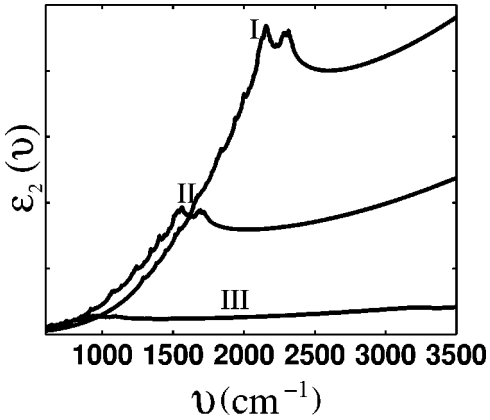

FIG. 7. The simulated absorption spectra including all three pockets of the indirect *L*-*T*-point transition in 30-nm-diam bismuth nanowires at room temperature shown for three values of the band overlap energies for bulk bismuth, at 300 K. Curves I, II, and III are for *L*-*T* band overlap energies of 172 (1387), 98 (790), and 24 (194) meV (cm^{-1}), respectively. The reported band overlap energy in bismuth at room temperature is 98 meV (790 cm^{-1}) (Ref. 9).

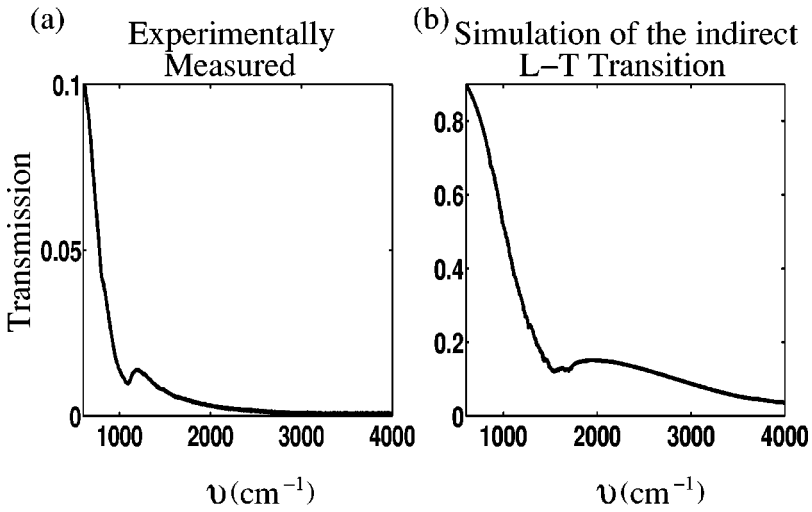

FIG. 8. (a) The measured optical transmission as a function of wave number of free-standing bismuth nanowires for the wave-number range of 650–4000 cm^{-1}. (b) The simulated optical transmission as a function of wave number resulting from an indirect L-T transition in bismuth nanowires with a diameter of 45 nm for the wave-number range of 650–4000 cm^{-1}. Note that the minimum transmission in the experimental spectra is at $\sim$1100 cm^{-1}, and in the simulated spectra is at $\sim$1500 cm^{-1}. The differences in the magnitude of the transmission likely result from the fact that only optical absorption from an indirect transition is simulated in (b), while in the experimental measurements, (a), many absorption and scattering mechanisms are likely to be present.

sensitive to the ratio of the effective masses of the L- and T-point pockets. When the T-point hole mass is decreased, the energy at which the L-point mass equals the T-point mass also decreases. Therefore, when the T-point mass decreases, the energy of the absorption peak downshifts. The simulations show that a decrease in the T-point hole effective mass by 10% results in a downshift of the absorption spectra by $\sim$75 cm^{-1}. Likewise, when the hole mass at the L point decreases, the energy at which the L-point mass equals the T-point mass increases, and the absorption peak occurs at a higher photon energy. A decrease in the L-point hole mass by 10% results in an upshift of the absorption spectra by $\sim$90 cm^{-1}. When both the electron (T-point) and hole (L-point) masses are increased, the effects cancel out and the absorption peak wave number remains relatively constant.

IV. COMPARISON BETWEEN MODEL CALCULATIONS AND EXPERIMENTAL RESULTS

The Bi nanowires used in this study are fabricated utilizing porous anodic alumina templates,[15,16] which serve as a host material for the nanowires. Since alumina is a wide-band-gap semiconductor, individual wires, which are fixed in place and spatially separated, are electrically isolated from each other. Porous anodic aluminum oxide templates are fabricated by anodizing aluminum sheets in an oxalic acid electrolyte. During this process, cylindrical pores 7–200 nm in diameter are self-assembled into a hexagonal array. The pore diameter and the distance between the pores can be controlled systematically by varying the anodization voltage and the electrolyte used.[17,18] The thickness of the alumina template determines the wire length, which can thus be controlled by the anodization time. The thicknesses of samples used in this study are 40–60 μm. The pores in the alumina templates are filled with Bi using a pressure-injection technique.[15] The wires used for the free-standing nanowire measurements had a wire diameter of 60 nm before the alumina template surrounding the wires was etched away using a phosphoric acid–chromium trioxide etch. Since an $\sim$7-nm oxide grows on the free-standing wires after the alumina is selectively etched away,[19] the inner bismuth portion of the free-standing wires is expected to have a diameter of around 45 nm and therefore is predicted to exhibit a semimetal-semiconductor transition at around 100 K. In this study, the alumina has been etched away and the wires are electrically isolated by a thin ($\sim$7 nm) bismuth oxide that forms during the etch.[19] In order to determine the contribution of the bismuth oxide on the absorption spectra, a bismuth film was evaporated onto a potassium bromide (KBr) window, annealed in an oxygen environment until the bismuth film was completely oxidized, and then its optical transmission was measured. The transmission of the bismuth oxide film did not have any features in the energy range of our experiment. The measured absorption of the bismuth wires etched from the alumina template is therefore assumed to result solely from the absorption of bismuth, and not from bismuth oxide. For this study, wires etched from the alumina template were chosen over the wires within the alumina template because the line shape of the absorption is important for this study. When the wires are inside the template, a reverse effective medium theory is used to obtain the dielectric function of the wires, but this process is indirect and might not deduce an accurate line shape of the absorption in the wires. By etching the wires from the alumina, sample inhomogeneities are added, but the true absorption line shape can be directly measured via transmission or reflection measurements.

The optical reflection $R(\nu)$ and transmission $T(\nu)$ were measured as a function of wavelength at room temperature using a Nicolet Magna-IR 860 spectrometer and a Nic-Plan IR Microscope. The microscope FTIR allows transmission and reflection measurements through a microscope stage and therefore enables measurements of samples smaller than 1 mm^2. Reflection and transmission data were taken in the infrared region from $600 < \nu < 4000$ cm^{-1} at 293 K using a gold film as a comparison standard. The resolution was 2 cm^{-1}.

Figure 8(a) shows the measured and Fig. 8(b) the simulated optical transmission of bismuth nanowires as a function of the wave number. The simulated absorption includes the absorption from all three L-point carrier pockets and is for a 45-nm-diam wire. The measured absorption is from an $\sim$45-nm-diam, undoped, wire. The transmission profiles for

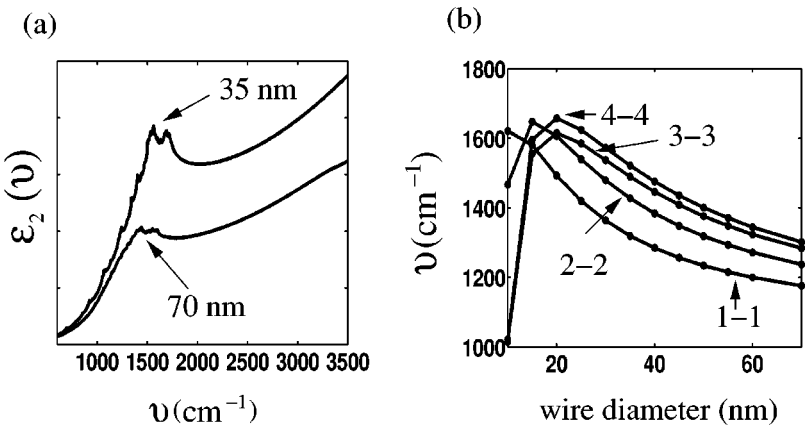

FIG. 9. (a) The simulated wave-number dependence of $\varepsilon_2(\nu)$ resulting from an indirect L-T transition in bismuth nanowires with a diameter of 70 and 35 nm for the wave-number range of 600–4000 cm^{-1}. The absorption peak in (a) moves from 1420 for the 70-nm wires to 1520 cm^{-1} for the 35-nm wires. This shift of $\sim$100 cm^{-1} is to be compared with the experimentally observed shift of 65 cm^{-1}. (b) The calculated energy difference measured in wave numbers between the first, second, third, and fourth subbands at the L-point valence band to the first, second, third, and fourth subbands at the T-point valence band.

the measured and simulated curves are very similar. As the light frequency is increased, the experimental /simulated transmission drops sharply and reaches a local minimum at around 1100 cm^{-1}/1500 cm^{-1} (0.136 eV/0.186 eV). The transmission then slightly increases, and finally steadily decays for the rest of the measured wave-number range. At 4000 cm^{-1}, the transmission is less than 10% of the transmission at 650 cm^{-1}. The measured transmission drops slightly faster and has slightly sharper features than the simulated curve. The differences in the magnitude of the transmission likely result from the fact that only optical absorption from an indirect transition is simulated in (b), while in the experimental measurements, (a), likely many absorption and scattering mechanisms are present. Furthermore, the magnitude of the experimentally measured transmission is affected by factors which are not measured, such as sample thickness and porosity. For example, the experimental transmission spectra of a different location on the same sample give a slightly different spectra, with a maximum transmission of $\sim$0.08 instead of $\sim$0.10, as presented in Fig. 8(a).

Although the simulated and measured spectra are similar, the local minimum in the transmission, which corresponds to a peak in the optical absorption, occurs at a higher photon energy in the simulated spectra than in the experimentally measured spectra. The transmission minimum in the simulated spectra occurs at $\sim$1520 cm^{-1} and in the measured spectra at $\sim$1100 cm^{-1}. This difference may result from approximations used in this calculation, inaccurate values of either the L- or T-point effective masses, inaccurate values of the band overlap energy of bulk bismuth at room temperature, or from a combination of these factors. If the L-point effective-mass tensor is taken to be larger or the T-point hole mass tensor smaller than the literature values, the wave number of the simulated absorption peak will decrease. The wave number of the simulated absorption peak will also decrease if the band overlap used in the simulations is decreased, see Fig. 7. Another possible explanation for the discrepancy is that the Lax two-band model may not completely hold for the energies contributing to the absorption spectra (up to 0.25 eV below the L-point midgap), because of possible contributions from bands outside of the two-band model for the L-point valence band.

In addition, the discrepancy between the energy of the simulated and measured absorption peaks may result in part from taking $s=0$ in Eq. (4). As shown in Fig. 4, when the lower-order subbands dominate the absorption spectra, the energy of the absorption peak decreases, yielding better agreement with experiment. When the lower-order subbands dominate the absorption spectra, not only does the energy of the absorption peak decrease, but the spectral width decreases as well, as shown in Fig. 4. Both the decrease in energy and the smaller spectral width of the absorption peak are in better agreement with experimental results when a nonzero value of s is used. The spectral width of the simulated absorption spectra results from contributions to the optical absorption from phonon emission and phonon absorption processes, the two types of L-point carrier pockets (A and B), wires with varying diameters, and contributions from different subbands. All four of these contributions increase the spectral broadening. Only considering the spectral peak broadening resulting from different subbands, a lower bound of the s value in Eq. (4) can be estimated to be 0.35. The dependence of the absorption spectra on s is discussed further in Ref. 20.

Small features in the experimental spectra are not reproduced in the simulated spectra, e.g., the weak absorption features near 750–800 cm^{-1} and at $\sim$600 cm^{-1} (more clearly shown in Ref. 1). These features are therefore attributed to an absorption mechanism other than an indirect L-T transition, such as intersubband transitions, and they are not discussed further in this paper.

Figure 9(a) shows the simulated absorption spectra resulting from an indirect L-T transition in bismuth nanowires with wire diameters of 70 and 35 nm. The wave number of the simulated absorption peak shifts from 1420 to 1520 cm^{-1}, because of the increased quantum confinement in the smaller diameter nanowires. The magnitude and sign of the shift (100 cm^{-1}) in the simulation agree well with the experimentally measured shift (65 cm^{-1}) when the wire diameter is varied from 35 nm to 60–80 nm.[6] The wave number of the peak in the absorption spectra is approximated by smoothing the simulated absorption spectrum. Figure 9(b) shows the calculated energy measured in wave numbers of the first, second, third, and fourth T-point subband edges to the first, second, third, and fourth L-point valence subband edges, respectively. The wave number of these transitions increases with decreasing wire diameter until a wire diameter of around 20 nm, at which point the wave numbers decrease.

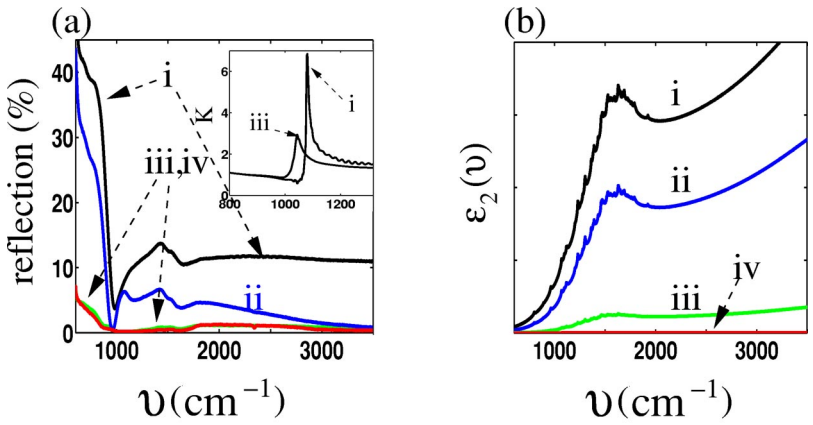

FIG. 10. (a) The measured wave-number dependence of the reflection of (i) nondoped, (ii) lightly *n*-type doped, (iii) medium *n*-type doped, and (iv) heavily *n*-type doped bismuth nanowires. The inset shows the calculated wave-number-dependent *K*, the imaginary part of the index of refraction of the (iii) medium and (i) undoped samples. (b) The simulated wave-number dependence of $\varepsilon_2(\nu)$ resulting from an indirect *L*-*T* transition in 40-nm-diam bismuth nanowires with (i) no doping, (ii) low *n*-type doping, (iii) medium *n*-type doping, and (iv) heavy *n*-type doping. In the experimental spectra, the reflection is decreased with the addition of *n*-type dopants, resulting from a decrease in the absorption. The simulated spectra also show a decrease in the absorption, reflected in the decrease in $\varepsilon_2(\nu)$, with increasing *n*-type dopant concentration.

For wires smaller than 20 nm, the effective mass at the *L* point is larger than the effective mass at the *T* point, and so the wave number of the *T*-*L*-point transition decreases with decreasing wire diameter.

In order to further test the identification of the absorption mechanism near 1000 cm^{-1}, the change in the simulated absorption with doping level is compared to previously measured Te-doped samples. The measured reflection as a function of wave number (for the same bismuth nanowire in alumina sample that was reported in Ref. 21) is shown in Fig. 10(a). These nanowire arrays have varying levels of *n*-type tellurium dopant concentrations. Normally for intrinsic materials, the absorption either stays constant or increases when dopants are added. In bismuth nanowires, however, the reflection decreases as the doping is increased. This corresponds to a decrease in the absorption, as seen in the relation

$$R=\frac{(1-n)^2+K^2}{(1+n)^2+K^2}, \tag{5}$$

where *R* is the reflection of an infinitely thick sample, *n* is the sample's index of refraction, and *K* is the imaginary part of the index of refraction. Figure 10(b) shows the simulated imaginary part of the dielectric function, $\varepsilon_2(\nu)$ (where $\varepsilon_2=2nK$), of bismuth nanowires with varying doping concentrations. The simulated results also show a decrease in absorption as the doping concentration increases. We can explain this decreased absorption by the predicted increased filling of the *T*-point valence band as the doping concentration increases, and hence the decrease in the number of final states to which electrons can be excited, see Fig. 5(b).

The energy of the absorption peak is slightly sensitive to the Fermi energy at room temperature. Since the peaks due to various subbands are separated by much less than the thermal energy, increasing the Fermi energy decreases the hole population in not just one, but in many of the *T*-point subbands. When the number of holes in a *T*-point subband is decreased, fewer electrons can be excited from the *L*-point to that *T*-point subband, and hence the absorption intensity resulting from this subband is decreased. From Fig. 5(b), we see that as the Fermi energy is increased, the *T*-point subbands contributing to the higher wave-number absorption are below the Fermi energy and those contributing to the lower wave-number absorption remain above the Fermi energy. Therefore, when the Fermi energy is slightly increased, the highest energy of the absorption peak downshifts slightly. When the Fermi energy is increased further, so that all the *T*-point hole subbands are completely submerged below the Fermi energy, no available states for the transition exist, and this absorption mechanism is quenched.

The downshift in the absorption peak energy with an increasing concentration of *n*-type dopants, as explained above, is not significant in the simulated spectra, since the energy shift is smaller than the spectral width of the simulated absorption peak.

Using Kramers-Kronig relations and a reverse effective medium theory,[1] the imaginary part of the index of refraction, *K*, as a function of wave number for the undoped and moderately doped nanowires is calculated from the reflection spectra. Since the transmission of the moderately doped sample is significant, this method only gives an approximate measure of the absorption spectra for this sample. The calculated results are shown in the inset of Fig. 10(a). Compared to the undoped sample, the doped sample has a decreased absorption intensity, as reflected in the decrease in *K*, as well as a slight ($\sim$40 cm^{-1}) decrease in the wave number of the peak in the absorption spectrum. This trend is qualitatively expected for absorption resulting from an indirect interband transition as described above, although it is not significant enough to observe in the simulated spectra at room temperature.

Although the shape of the absorption spectra and the polarization, wire diameter, and doping dependences are all explained by absorption resulting from the *L*-*T*-point indirect transition, the temperature dependence of this absorption

peak is not well explained. In bismuth, the absorption from many mechanisms (e.g., free carriers, intersubband, indirect interband, and direct interband transitions) is expected to change drastically with temperature. This results from the large temperature dependence of the effective mass, *L*-point band gap, *T*-point to *L*-point band overlap, and the free-carrier concentration.[8,9,22] However, preliminary results show only slight changes in the optical absorption when the temperature is varied between 400 K and 150 K. The small observed temperature dependence of the optical absorption is not explained by either intersubband absorption or indirect optical-absorption processes. The temperature dependence of the absorption spectra is further discussed in Ref. 20. In addition, Ref. 20 also discusses spectral broadening and the expected intensity of an absorption peak resulting from a phonon exchange mechanism, as expected for an indirect transition in bismuth nanowires.

V. CONCLUSIONS

This paper presents a numerical simulation of the optical absorption resulting from an electron excitation between the *L*- and *T*-point valence bands. Experimentally measured transmission spectra are compared to the simulated transmission spectra, and good agreement is obtained, as shown in Fig. 8. The similarity between these spectra strongly indicates that the measured absorption is dominated by this indirect electronic transition. Furthermore, the polarization dependence, the energy increase with decreasing wire size, the decrease in absorption intensity with increasing *n*-type doping levels, and the location of the absorption peak of the experimental curve are all consistent with the simulated spectra. The 400-cm^{-1} wave-number difference between the experimental and simulated peak is not yet understood and needs further investigation, although several explanations are proposed. Detailed temperature-dependent studies are needed to gain further understanding. Two possible mechanisms, a spatial derivative in the vector potential and surface defects, are proposed for the momentum transfer required for the observation of an indirect transition.

ACKNOWLEDGMENTS

The authors greatly appreciate the useful discussions with Dr. Gene Dresselhaus, Oded Rabin, Dr. J. Heremans, Shin Grace Chou, and Wolfgang Porod. In addition, we appreciate Karlene Maskala's and Professor Yoel Fink's help in fabricating the 200-nm alumina oxide sample. The authors also acknowledge NSF Grant No. DMR-01-16042, U.S. Navy, Contract No. N00167-98-K0024, ONR Grant No. N00014-02-1-0865, MURI Subcontract No. 0205-G-BB853, and Intel for financial support. This work made use of MRSEC Shared Facilities supported by the National Science Foundation Contract No. DMR-9400334.

*Now at Los Alamos National Laboratory, Los Alamos, NM 87545. Electronic address: mblack@lanl.gov

[1] M.R. Black, Y.-M. Lin, S.B. Cronin, O. Rabin, and M.S. Dresselhaus, Phys. Rev. B **65**, 195417 (2002).

[2] G. Dresselhaus, M.S. Dresselhaus, Z. Zhang, X. Sun, J. Ying, and G. Chen, in *Seventeenth International Conference on Thermoelectrics: Proceedings, ICT'98; Nagoya, Japan*, edited by K. Koumoto (Institute of Electrical and Electronics Engineers, Piscataway, NJ, 1998), pp. 43–46.

[3] R.T. Isaacson and G.A. Williams, Phys. Rev. **185**, 682 (1969).

[4] Y.-M. Lin, S.B. Cronin, J.Y. Ying, M.S. Dresselhaus, and J.P. Heremans, Appl. Phys. Lett. **76**, 3944 (2000).

[5] Y.-M. Lin, X. Sun, and M.S. Dresselhaus, Phys. Rev. B **62**, 4610 (2000).

[6] M.R. Black, M. Padi, S.B. Cronin, Y.-M. Lin, O. Rabin, T. McClure, G. Dresselhaus, P.L. Hagelstein, and M.S. Dresselhaus, Appl. Phys. Lett. **77**, 4142 (2000).

[7] O. Madelung, in *Landolt–Börnstein Numerical Data and Functional Relationships in Science and Technology, New Series*, edited by K.-H. Hellwege (Springer-Verlag, Berlin, 1982), Vol. 17a, pp. 43–87.

[8] M.P. Vecchi and M.S. Dresselhaus, Phys. Rev. B **10**, 771 (1974).

[9] C.F. Gallo, B.S. Chandrasekhar, and P.H. Sutter, J. Appl. Phys. **34**, 144 (1963).

[10] B. Lax and J.G. Mavroides, in *Advances in Solid State Physics* (Academic Press, New York, 1960), Vol. 11.

[11] T. Miller, E.D. Hansen, W.E. McMahon, and T.C. Chiang, Surf. Sci. **376**, 32 (1997).

[12] B. Feuerbacher, B. Fitton, and R.F. Willis, in *Photoemission and the Electronic Properties of Surfaces* (John Wiley and Sons, New York, NY, 1978).

[13] P. Enders and R. Schuchardt, Phys. Status Solidi B **135**, 207 (1986).

[14] B. Lax, J.G. Mavroides, H.J. Zeiger, and R.J. Keyes, Phys. Rev. Lett. **5**, 241 (1960).

[15] Z. Zhang, J. Ying, and M. Dresselhaus, J. Mater. Res. **13**, 1745 (1998).

[16] J. Heremans, C.M. Thrush, Y. Lin, S. Cronin, Z. Zhang, M.S. Dresselhaus, and J.F. Mansfield, Phys. Rev. B **61**, 2921 (2000).

[17] J.W. Diggle, T.C. Downie, and C.W. Goulding, Chem. Rev. (Washington, D.C.) **69**, 365 (1969).

[18] J.P. Sullivan and G.C. Wood, Proc. R. Soc. London, Ser. A **317**, 511 (1970).

[19] S.B. Cronin, Y.-M. Lin, P.L. Gai, O. Rabin, M.R. Black, G. Dresselhaus, and M.S. Dresselhaus, in *Anisotropic Nanoparticles: Synthesis, Characterization and Applications: MRS Symposium Proceedings, Boston, 2000*, edited by S. Stranick, P.C. Searson, L.A. Lyon, and C. Keating (Materials Research Society Press, Pittsburgh, 2001), pp. C571–C576.

[20] Marcie R. Black, Ph.D. thesis, Massachusetts Institute of Technology, Department of Electrical Engineering and Computer Science, 2003.

[21] M.R. Black, K.R. Masklay, O. Rabin, Y.-M. Lin, S.B. Cronin, M. Padi, Y. Fink, and M.S. Dresselhaus, in *Nanophase and Nanocomposite Materials IV: MRS Symposium Proceedings, Boston, 2001*, edited by S. Komarneni, R.A. Vaia, G.Q. Lu, J.-I. Matsushita, and J.C. Parker (Materials Research Society Press, Pittsburgh, 2002), p. AA8.9.

[22] V. Damodara Das and N. Soundararajan, Phys. Rev. B **35**, 5990 (1987).